Nanoscale

Cite this: *Nanoscale*, 2011, **3**, 3244

www.rsc.org/nanoscale

**PAPER**

# Striped nanowires and nanorods from mixed SAMS†

**Chetana Singh,[a] Ying Hu,[b] Bishnu P. Khanal,[c] Eugene R. Zubarev,[c] Francesco Stellacci[b] and Sharon C. Glotzer*[ad]**

***Received 26th February 2011, Accepted 13th May 2011***
**DOI: 10.1039/c1nr10215j**

We investigate the use of mixed self-assembled monolayers (SAMs) for creating nanoscale striped patterns on nanowires and nanorods. Our simulations predict that SAMs comprised of an equal composition of length-mismatched, thermodynamically incompatible surfactants adsorbed on nanowire surfaces self-organize into equilibrium stripes of alternating composition always perpendicular, rather than parallel, to the nanowire axis. We support the simulation results with preliminary experimental investigations of gold nanorods coated with binary mixtures of ligand molecules, which show stripes roughly perpendicular to the rod axis in all cases.



Patchy particles with attractive, repulsive or reactive patterns on the surface are important as building blocks for self-assembly.[1–4] Nanoscale surface patterns also impart to nanoparticles remarkable catalytic,[5] biological[6] and wetting properties[7,8] unique to the nanoscale. Patchy particles of many shapes have been demonstrated, with controlled patterns obtained through different methods including deposition of gold on, *e.g.*, spheres,[9–12] rods,[13,14] and tetrapods,[13] electrohydrodynamic co-jetting,[15,16] microcontact printing[17] and self-assembly of mixed ligand SAMs on gold and silver nanospheres.[18–20] Ordered patterns on nanowires and nanorods are of particular interest for potential fabrication of multisegmented[21,22] nanorods and nanowires *via* self-assembly. Multisegmented nanowires, usually fabricated using sequential electrochemical deposition, have applications in the fields of molecular recognition, biosensing, multiplexed detection, microelectronics, catalysis, information storage and tagging (bar-coded nanorods).[23–32] Here we demonstrate that mixed SAMs adsorbed on nanorod or nanowire surfaces form striped patterns that alternate along the length of the rod/wire, and always form perpendicular to the rod/wire axis. Although further development is required to exploit this patterning phenomenon for the applications of multisegmented wires, our study provides the first demonstration that mixed SAMs can be used to pattern nanorods and nanowires through self-assembly.

We use dissipative particle dynamics (DPD) simulations[33] to simulate the microphase separation behavior of a mixed SAM of long and short surfactants grafted *via* identical head groups to a cylindrical surface. Equal numbers of both surfactants are used, and distributed randomly around the cylinder at time $t = 0$. Each surfactant is modeled as a bead-spring chain in which consecutive DPD beads are connected by simple harmonic springs. Simple bead-spring models are commonly used to study properties of polymer and surfactant molecules and have successfully predicted the phase behavior of these molecules in the past.[33–37] The DPD conservative force is a soft and purely repulsive force. The incompatibility between two species is modeled by making dissimilar beads more repulsive than similar beads. The source of this incompatibility is the attraction of both species to the solvent molecules, which are treated implicitly in the DPD model and method.[33] The parameters used here correspond to water as the solvent. To simulate the behavior in other solvents, parameters for effective potentials can be calculated starting from atomistic molecular dynamics simulations.[33,38] The excess repulsion $\Delta a$ can be increased to make the two species more incompatible. The length difference, $\Delta l$, between surfactants is measured as the difference in the number of beads comprising the surfactant chains. All lengths are measured in units of $\sigma$, the diameter of a single DPD bead. We use a reduced temperature $k_BT = 1$, and a reduced time step $\tau = 0.02$. Each bead-spring surfactant contains a single-bead head group and a tail. The head group is constrained to move on the cylinder surface using constrained dynamics.[34] Periodic boundary conditions are used along the length of the cylinder. Additional details on the use of this method to simulate self-assembly of mixed ligand SAMs on spherical nanoparticles may be found in ref. 20 and 39. For the experimental studies, we synthesize gold nanorods using methods described in the literature,[40] and coat the rods with a mixed SAM of octanethiol and mercaptopropionic acid *via* place exchange reactions (details in

[a]*Department of Chemical Engineering, University of Michigan, Ann Arbor, Michigan, USA. E-mail: sglotzer@umich.edu*
[b]*Department of Materials Science and Engineering, MIT, Cambridge, Massachusetts, USA*
[c]*Bioscience Research Collaborative and Department of Chemistry, Rice University, Houston, Texas, 77005, USA*
[d]*Department of Materials Science and Engineering, University of Michigan, Ann Arbor, Michigan, USA*
† Electronic supplementary information (ESI) available. See DOI: 10.1039/c1nr10215j

the ESI†). The rods are drop cast onto gold substrates and imaged with scanning tunneling microscopy (STM) according to previously discussed approaches.[41–43]

Fig. 1 shows examples of striped nanowires and nanorods that we obtained in simulations and experiments. Experimental images (b–e) show nanorods coated with various stoichiometric mixtures of the ligands. As in nanoparticle imaging, observing clear and reproducible structure on nanorods is contingent on the tip imaging condition, sample preparation and imaging feedback. We observed only a few examples of rods (~20%) that present a ligand shell clean enough to show a clear structure, yet in those cases we observed clear and reproducible stripe-like structures (Fig. 1). In all cases, the observed stripes are perpendicular to the rod axis. In Fig. 1(c) and (e), we show two of a series of 21 images of the same nanorod captured at different tip speeds, varying from 0.17 μm $s^{-1}$ to 2.0 μm $s^{-1}$. As found for spherical nanoparticles, we find limited to no dependence of stripe width on tip speed[42] (Fig. S1†). We note that stripes in this rod are very clear and can be imaged across a tip-speed range wider than that for spherical particles. This wider range may be attributed to many factors (among them cleanness of the sample, and more resistance to sample drag/vibration/rotation while imaging due to increased inertia) but may also be due to formation of more clearly defined and ordered stripes on nanorods as compared to nanoparticles, which make them easier to observe. In Fig. S2(a) and (d)†, we show individual end groups of the ligands and in Fig S2 (b) and (c)†, we show stripe-like structures. This demonstrates that the "stripes" are composed of individual end groups.

The nanorod diameters (including the width of the octanethiol coating) observed in our imaging sessions and samples varied from 3 nm to 12 nm. Stripe-like structures were consistently observed through different speeds on nanorods 3.6 nm (Fig. 1(b)) and 4.2 nm wide (Fig. 1(c)). The extended length of octanethiol is around 1.1 nm, so these nanorods are calculated to be between 1.4 nm and 2 nm wide. Finally, we find that the widths of the domains (0.75 nm ± 0.1 nm) are commensurate with those seen on spherical nanoparticles.[19,43]

Recently, we showed that striped patterns may be obtained on spherical nanoparticles coated with mixed SAMs of incompatible surfactants.[18,19,43] Stripes form *via* microphase separation when one of the two incompatible surfactants is sufficiently longer or bulkier than the other.[20] By creating additional interfaces where long surfactants are adjacent to short ones, the system is penalized energetically relative to macrophase separation, but gains conformational entropy in the ability of the long surfactants to bend over neighboring short surfactants[20] (Fig. 2(a) and (b)). The

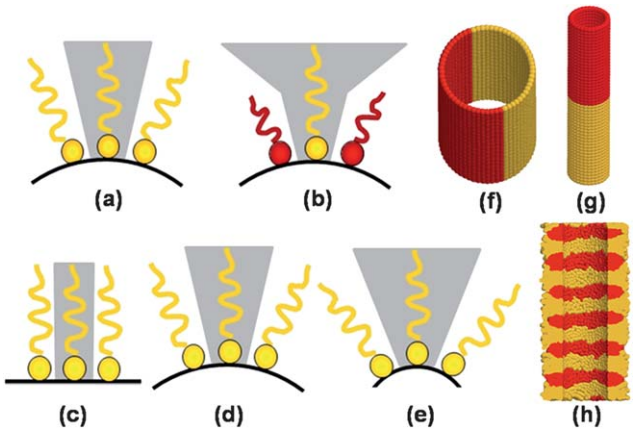


**Fig. 2** (a) and (b) Schematic showing how the free volume (grey, shaded area) and hence conformational entropy of a long surfactant chain increases when it is surrounded by shorter chains as compared to chains of the same length. (c)–(e) Cartoons depicting the approximate free volume (grey, shaded area) available to a single surfactant tail in the presence of neighboring ligands on substrates of decreasing radii of curvature from left to right. Patterns that can form by phase separation of simple incompatible mixtures on cylindrical surfaces: (f) macrophase separation resulting in interfaces parallel to the cylinder axis and (g) macrophase separation resulting in interfaces perpendicular to the cylinder axis. (h) Cross-sectional view of microphase separation resulting in stripes for mixtures of long (yellow) and short (red) surfactants (surfactant tails on the front half of the cylinder have been removed to reveal the bending of long surfactants over the shorter ones).

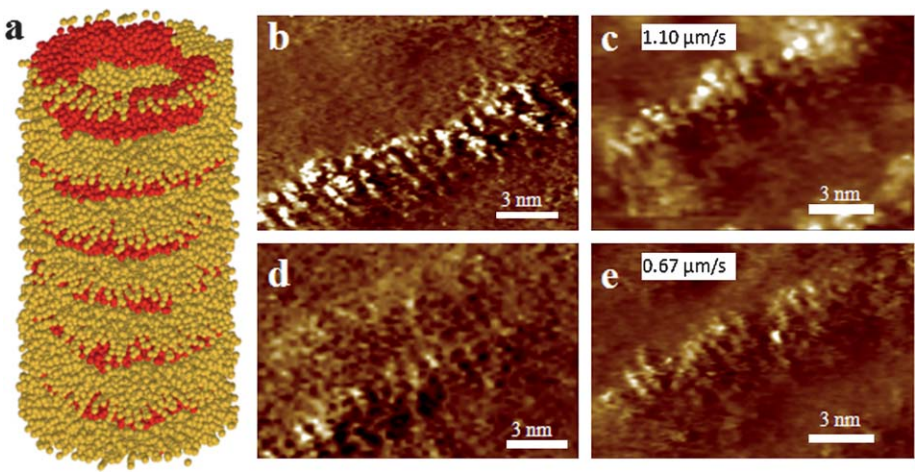


**Fig. 1** (a) Striped nanowire obtained in computer simulations of long (yellow) and short (red) incompatible bead-spring chains. Images (b)–(d) show three different rods with average stripe widths of 0.87 nm, 0.77 nm and 0.99 nm, respectively. Images (c) and (e) are images of the same rod captured at different tip speeds. Limited to no dependence of the stripe width on tip speed was found (Fig. S1†).

preference of a long surfactant to be next to a shorter one can also be demonstrated by counting the number of states available to a surfactant when surrounded by long or short surfactants and associating the number of available states to its conformational entropy.[44] We recently found that mixed SAMs on flat surfaces behave similarly, resulting in striped and worm-like microphase separated domains under suitable conditions.[45] If the length mismatch is insufficient to create enough conformational entropy to offset the increased energy of the system arising from the interfaces, then on both spherical and flat surfaces macrophase separation occurs whereby the SAM phase separates into two coexisting phases rich in one or the other ligand, with a single interface. As for spherical surfaces, the free volume and thus conformational entropy gain in the creation of additional interfaces becomes increasing less important as the radius of curvature of the substrate decreases.[20,39] Fig. 2(c)–(e) show cartoons of the increased free volume as the radius of curvature of the substrate is decreased.

For a mixture of incompatible but otherwise similar ligands confined to the surface of a cylinder, macrophase separation can lead to formation of an interface either parallel to, or perpendicular to, the cylinder axis, as shown in Fig. 2(f) and (g), based on the aspect ratio of the cylinder. When the ratio of the circumference $2\pi R_C$ to the length $L$ of the cylinder is small (large), the interfaces between macrophase-separated domains form parallel to (perpendicular to) the cylindrical axis so as to minimize the total interface length. Fig. 1(a) and 2(h) show that mixtures of long and short incompatible surfactants create additional interfaces, forming stripes on cylindrical surfaces as on spherical nanoparticles. The bending of long surfactants over the short ones to gain conformational entropy is shown schematically in Fig. 2(b) and demonstrated in Fig. 2(h).

We find both in our simulations and experiments that the stripes form always perpendicular to the axis of the wire/rod. The robustness of the perpendicular stripes, or rings, can be explained by considering the potential conformational entropy gain of the long surfactants arranged in stripes perpendicular *vs.* parallel to the cylinder axis (Fig. 3). When stripes form perpendicular to the axis of the cylinder (Fig. 3(a)), the long surfactants enjoy the maximum possible conformational entropy because of the increased free volume along the circumference of the cylinder due to the surface curvature, and that along the length of the cylinder due to the bending of long surfactants over neighboring short surfactants. In contrast, when stripes are parallel to the cylinder axis (Fig. 3(b)), no free volume or conformational entropy gain is possible along the length of the cylinder and crowding of the long surfactants occurs in that direction. Therefore, for the same stripe width, rings perpendicular to the cylinder axis are always entropically favored over stripes along the cylinder length. Helices with a short pitch are the next best configuration after rings in terms of system free energy. In multiple simulations performed for the same surfactant system, we rarely, if ever, observe helices instead of separated stripes. Since their occurrence is rare and the pitch short, we believe that they are kinetically arrested structures or defective rings. The difference in the free energies of rings and helices is expected to be very small, so much so that it would take very long simulation times for helices to relax into the equilibrium ring structures. We note that the unique ability of a cylindrical surface to align stripes

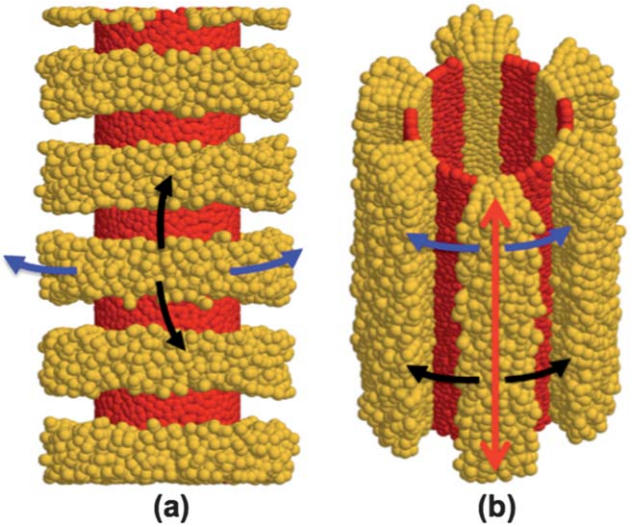


**Fig. 3** Directions in which the free volume and conformational entropy can be gained by the long (yellow) surfactants when stripes are formed (a) perpendicular to, and (b) parallel to the cylindrical axis. Tails of the short (red) surfactants have been removed for clarity. Blue arrows indicate the direction in which the long surfactants gain free volume due to the curvature of the substrate. Black arrows indicate the direction in which the long surfactants gain free volume by bending over the neighboring short surfactants. Red arrows indicate the direction in which crowding of the long surfactants occurs.

perpendicular to the axis can also be exploited to modify patterns formed in SAMs on flat surfaces.[46] The direction of the stripes may become inconsequential for very wide cylinders when the radius of curvature is practically infinite. Wide cylinders are nearly equivalent to flat substrates with no distinction between the length and the circumference. Spheres on the other hand have the same curvature in all directions and will therefore not promote stripes along any preferred direction. Cylinders are therefore unique and interesting with respect to their unidirectional curvature.

As we found previously for mixed SAMs on spherical nanoparticles,[20,39] the striped patterns depend on the degree of incompatibility and length difference between the two species. Fig. 4 shows the effect of increasing the incompatibility ($\Delta a$) between the surfactants. For weakly incompatible surfactant tails, irregularly shaped microphase-separated domains form (Fig. 4(a)). The average equilibrium pattern is stable, and the ligands move constantly between domains. On increasing the incompatibility, striped domains perpendicular to the cylinder axis appear (Fig. 4(b)). The width of these stripes or rings increases somewhat as the incompatibility is further increased (Fig. 4(c)–(e).) For strongly incompatible mixtures, macrophase separation occurs (Fig. 4(f)).

Fig. 5 shows the effect of increasing surfactant length difference on phase separation. Mixtures of surfactants with equal lengths, *i.e.* $\Delta l = 0$ (Fig. 5(a)), or small $\Delta l$ (Fig. 5(b)) show macrophase separation. We have ascertained on longer cylinders that the patterns shown in Fig. 5(a) and (b) are not wide and repeating stripes but rather macrophase-separated surfactants. For these mixtures the gain in conformational entropy resulting from microphase separation is either absent or insufficient to

 

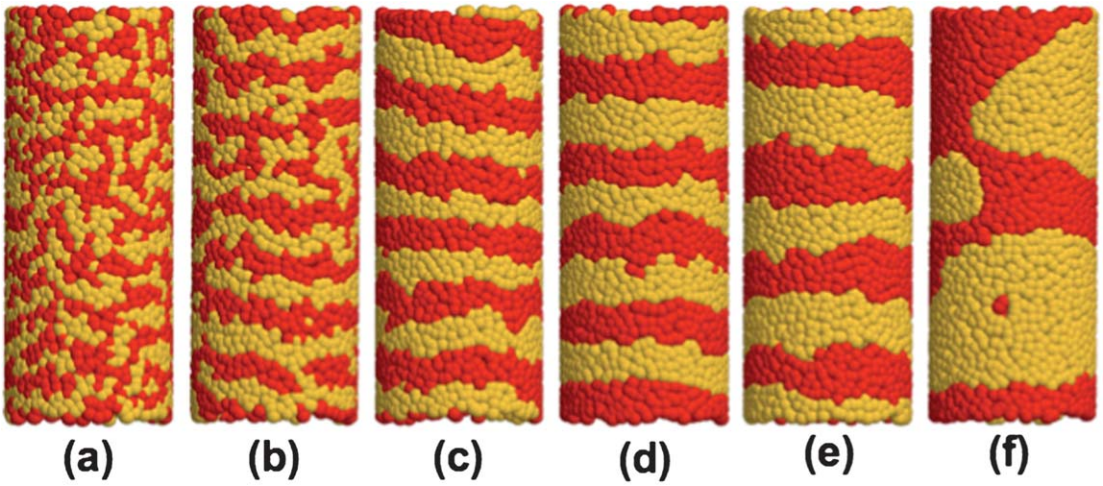


**Fig. 4** Patterns formed by long (7-bead, yellow) and short (4-bead, red) surfactants with increasing incompatibility ($\Delta a$). Values of $\Delta a$, from left to right, are: (a) 3, (b) 5, (c) 10, (d) 15, (e) 20 and (f) 25. Surfactant tails have been removed for clarity.

overcome the enthalpic penalty of forming interfaces. Therefore energetic interactions dominate and interface-minimizing macrophase separation occurs. On increasing $\Delta l$, stripes appear, again perpendicular to the cylinder axis (Fig. 5(c)–(f).) We find the dependence of stripe width on $\Delta l$ is weaker than the dependence on $\Delta a$ (Fig. 4) for the surfactant lengths considered here. We observe interesting behavior at the limits of small and large cylinder radii, $R_C$ (Fig. 6). On very narrow cylinders, the SAM macrophase separates, leading to the formation of biphasic or bisegmented nanorods (Fig. 6(a)), analogous to Janus nanoparticles formed by binary SAMs on spherical surfaces.[39] This is the first prediction of "Janus rods" or "Janus wires" for mixed SAMs. As the cylinder diameter increases for fixed $\Delta l$ and $\Delta a$, stripes appear, with decreasing stripe width as $R_C$ increases (Fig. 6(b)–(e)). For sufficiently large $R_C$, the stripe width reaches a self-limiting value (Fig. 6(e)–(g)) when the tails of the long surfactants in neighboring stripes interact in the region above the shared short surfactant stripe, reducing the conformational entropy advantage and preventing further narrowing of the stripes. A plot of the inverse stripe width for increasing $R_C$ is provided in Fig. 6(h). We find that the length of the cylinders does not influence stripe formation (see ESI, Fig. S3†). Stripes of different widths commensurate with the cylinder length and circumference were also found to be unstable and always formed rings of the preferred width around the cylinder (see ESI, Fig. S4†).

The formation of biphasic, or Janus, nanowires for very narrow cylinders (Fig. 6(a)) can be understood based on the free volume available to a long surfactant tail grafted on surfaces of varying radii of curvature (Fig. 2(c)–(e)). For large to moderate width cylinders (Fig. 2(c) and (d)), the free volume associated with the surfactant tail arising from the surface curvature is minimal, and interfaces (microphase separation) are required for the long surfactants to maximize their entropy while overall minimizing the system free energy. For very narrow cylinders (Fig. 2(e)), a large free volume, and hence conformational entropy, is available to a surfactant tail from the surface curvature alone, irrespective of the phase-separated pattern. Hence

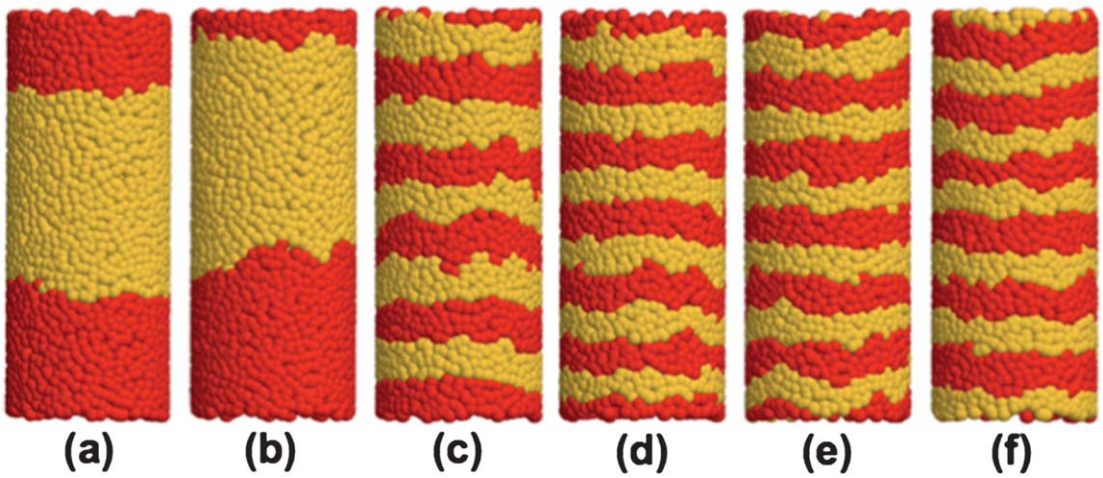


**Fig. 5** Patterns formed by long (yellow) and short (red) surfactants as their length difference, $\Delta l$, increases. The length of the short surfactant is kept fixed at 4 beads. Values of $\Delta l$ from left to right are: (a) 0, (b) 2, (c) 3, (d) 5, (e) 7 and (f) 9. Surfactant tails have been removed for clarity.

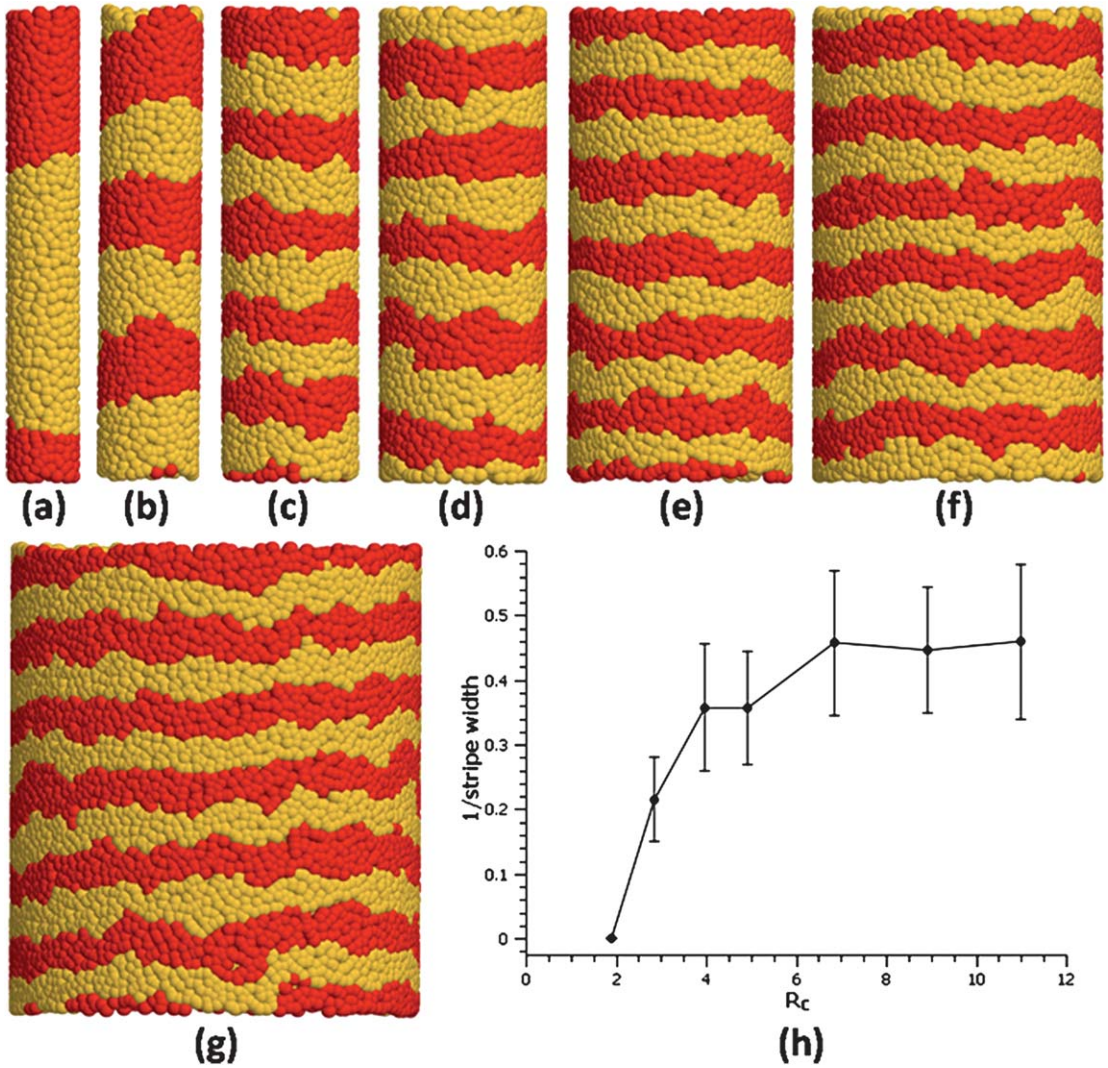


**Fig. 6** (a)–(g) Patterns formed by long (7-bead, yellow) and short (4-bead, red) surfactants as the cylinder radius, $R_C$, is increased. Values of $R_C$ from left to right are: (a) 2, (b) 3, (c) 4, (d) 5, (e) 7, (f) 9 and (g) 11. Surfactant tails have been removed for clarity. (h) Plot of inverse stripe width (long surfactants) *vs.* $R_C$. Error bars indicate the standard deviation.

additional interfaces are unnecessary for small radii of curvature, and macrophase separation results in biphasic nanowires.

Among phase separating mixtures with competing interactions confined to cylindrical surfaces, the system of incompatible, unlike point charges has been most extensively studied.[47–51] Microphase separation in that system results from competing short-range attractions that drive macrophase separation at low $T$ and long-range electrostatic interactions that drive mixing. Comparison of microphase-separated patterns formed by that system and ours reveals several key differences. For example, in the system of incompatible, unlike point charges, stripes perpendicular or parallel to the cylinder axis as well as stable helical stripes may form while in our system we observe only rings perpendicular to the axis.[50] Defect-mediated stripes are also seen in the charged system while defects in our system appear only when the surfactants are highly incompatible or the surface coverage is very high (results not shown), both of which slow the phase separation process so that equilibrium structures are difficult to access in the time scale of the simulation. Another important difference is that in the charged system, patterns varying from helices to rings form on narrow cylinders[47,48] and macrophase separation occurs at very small radii.[47] In our system, only macrophase separation occurs on narrow cylinders, for reasons described above. Thus the rich variety of patterns predicted for systems of incompatible, charged particles is not seen in phase separating mixed SAMs on cylindrical surfaces. Instead, the perpendicular stripe patterns (rings) appear to be robust for a wide range of conditions. This robustness may be exploited for many applications.

A variety of patterns, ranging from patches or micelles to stripes, has been observed for several decades now in numerous systems phase separating on flat surfaces.[52–65] Driving forces include electrostatic attraction/repulsion, incompatibility, length or bulkiness difference between molecules, reactivity, chemical bonding and difference in magnetization. The uniqueness of the cylindrical substrate lies in the fact that the anisotropy of the cylindrical shape breaks the symmetry and helps align stripes (Fig. 3 and ref. 46).

 

In conclusion, our simulations predict and preliminary experiments confirm that mixed SAMs can be used to obtain nanoscale, ordered, striped patterns on the surface of nanowires and nanorods. Due to the strong entropic preference for the formation of alternating rings of the two different surfactants around the cylinders, as compared to formation of stripes along the cylinder length, nearly defect-free rings are obtained in simulations as well as experiments. Surfactants with varying degrees of incompatibility and different length differences can be chosen to tune the stripe width, providing a simple and robust method for patterning nanorods and nanowires.

CS and SCG acknowledge funding from the National Science Foundation under NIRT grant CTS-0403633. CS acknowledges a University of Michigan Rackham Graduate School Predoctoral Fellowship. FS acknowledges an NSF CAREER award and the Packard Foundation for support. We thank Dr Kevin Kohlstedt for his comments on the manuscript. This material is based upon work supported by the DOD/DDRE under award no. N00244-09-1-0062 (SCG). E.R.Z. acknowledges financial support by NSF (DMR-0547399) and the Robert A. Welch Foundation (C-1703). Any opinions, findings, and conclusions or recommendations expressed in this publication are those of the author(s) and do not necessarily reflect the views of the DOD/DDRE. We thank the UM Center for Advanced Computing for support of our computer cluster.

## References


1 S. C. Glotzer, Some assembly required, *Science*, 2004, **306**(5695), 419–420.
2 S. C. Glotzer and M. J. Solomon, Anisotropy of building blocks and their assembly into complex structures, *Nat. Mater.*, 2007, **6**, 557–562.
3 Z. L. Zhang and S. C. Glotzer, Self-assembly of patchy particles, *Nano Lett.*, 2004, **4**(8), 1407–1413.
4 Z. L. Zhang, M. A. Horsch, M. H. Lamm and S. C. Glotzer, Tethered nano building blocks: toward a conceptual framework for nanoparticle self-assembly, *Nano Lett.*, 2003, **3**(10), 1341–1346.
5 S. G. Penn, L. He and M. J. Natan, Nanoparticles for bioanalysis, *Curr. Opin. Chem. Biol.*, 2003, **7**(5), 609–615.
6 A. Verma, O. Uzun, Y. H. Hu, Y. Hu, H. S. Han, N. Watson, S. L. Chen, D. J. Irvine and F. Stellacci, Surface-structure-regulated cell-membrane penetration by monolayer-protected nanoparticles, *Nat. Mater.*, 2008, **7**(7), 588–595.
7 A. Centrone, E. Penzo, M. Sharma, J. W. Myerson, A. M. Jackson, N. Marzari and F. Stellacci, The role of nanostructure in the wetting behavior of mixed-monolayer-protected metal nanoparticles, *Proc. Natl. Acad. Sci. U. S. A.*, 2008, **105**(29), 9886–9891.
8 J. J. Kuna, K. Voitchovsky, C. Singh, H. Jiang, S. Mwenifumbo, P. K. Ghorai, M. M. Stevens, S. C. Glotzer and F. Stellacci, The effect of nanometre-scale structure on interfacial energy, *Nat. Mater.*, 2009, **8**(10), 837–842.
9 A. B. Pawar and I. Kretzschmar, Patchy particles by glancing angle deposition, *Langmuir*, 2008, **24**(2), 355–358.
10 A. B. Pawar and I. Kretzschmar, Fabrication, assembly, and application of patchy particles, *Macromol. Rapid Commun.*, 2010, **31**(2), 150–168.
11 G. Zhang, D. Y. Wang and H. Moehwald, Nanoembossment of Au patterns on microspheres, *Chem. Mater.*, 2006, **18**(17), 3985–3992.
12 G. Zhang, D. Y. Wang and H. Mohwald, Decoration of microspheres with gold nanodots-giving colloidal spheres valences, *Angew. Chem., Int. Ed.*, 2005, **44**(47), 7767–7770.
13 T. Mokari, E. Rothenberg, I. Popov, R. Costi and U. Banin, Selective growth of metal tips onto semiconductor quantum rods and tetrapods, *Science*, 2004, **304**(5678), 1787–1790.
14 T. Mokari, C. G. Sztrum, A. Salant, E. Rabani and U. Banin, Formation of asymmetric one-sided metal-tipped semiconductor nanocrystal dots and rods, *Nat. Mater.*, 2005, **4**(11), 855–863.
15 K. H. Roh, D. C. Martin and J. Lahann, Biphasic Janus particles with nanoscale anisotropy, *Nat. Mater.*, 2005, **4**(10), 759–763.
16 K. H. Roh, D. C. Martin and J. Lahann, Triphasic nanocolloids, *J. Am. Chem. Soc.*, 2006, **128**(21), 6796–6797.
17 O. Cayre, V. N. Paunov and O. D. Velev, Fabrication of asymmetrically coated colloid particles by microcontact printing techniques, *J. Mater. Chem.*, 2003, **13**(10), 2445–2450.
18 G. A. DeVries, M. Brunnbauer, Y. Hu, A. M. Jackson, B. Long, B. T. Neltner, O. Uzun, B. H. Wunsch and F. Stellacci, Divalent metal nanoparticles, *Science*, 2007, **315**, 358–361.
19 A. M. Jackson, J. W. Myerson and F. Stellacci, Spontaneous assembly of subnanometre-ordered domains in the ligand shell ofmonolayer-protected nanoparticles, *Nat. Mater.*, 2004, **3**(5), 330–336.
20 C. Singh, P. K. Ghorai, M. A. Horsch, A. M. Jackson, R. G. Larson, F. Stellacci and S. C. Glotzer, Entropy-mediated patterning of surfactant-coated nanoparticles and surfaces, *Phys. Rev. Lett.*, 2007, **99**(22), 226106-1.
21 S. J. Hurst, E. K. Payne, L. D. Qin and C. A. Mirkin, Multisegmented one-dimensional nanorods prepared by hard-template synthetic methods, *Angew. Chem., Int. Ed.*, 2006, **45**(17), 2672–2692.
22 M. E. Pearce, J. B. Melanko and A. K. Salem, Multifunctional nanorods for biomedical applications, *Pharm. Res.*, 2007, **24**, 2335–2352.
23 R. M. Hernandez, L. Richter, S. Semancik, S. Stranick and T. E. Mallouk, Template fabrication of protein-functionalized gold-polypyrrole-gold segmented nanowires, *Chem. Mater.*, 2004, **16**(18), 3431–3438.
24 C. D. Keating and M. J. Natan, Striped metal nanowires as building blocks and optical tags, *Adv. Mater.*, 2003, **15**(5), 451–454.
25 J. H. Lee, J. H. Wu, H. L. Liu, J. U. Cho, M. K. Cho, B. H. An, J. H. Min, S. J. Noh and Y. K. Kim, Iron-gold barcode nanowires, *Angew. Chem., Int. Ed.*, 2007, **46**, 3663–3667.
26 F. Liu, J. Y. Lee and W. J. Zhou, Template preparation of multisegment PtNi nanorods as methanol electro-oxidation catalysts with adjustable bimetallic pair sites, *J. Phys. Chem. B*, 2004, **108**(46), 17959–17963.
27 F. Liu, J. Y. Lee and W. J. Zhou, Segmented Pt/Ru, Pt/Ni, and Pt/RuNi nanorods as model bifunctional catalysts for methanol oxidation, *Small*, 2006, **2**(1), 121–128.
28 S. R. Nicewarner-Pena, A. J. Carado, K. E. Shale and C. D. Keating, Barcoded metal nanowires: optical reflectivity and patterned fluorescence, *J. Phys. Chem. B*, 2003, **107**(30), 7360–7367.
29 S. R. Nicewarner-Pena, R. G. Freeman, B. D. Reiss, L. He, D. J. Pena, I. D. Walton, R. Cromer, C. D. Keating and M. J. Natan, Submicrometer metallic barcodes, *Science*, 2001, **294**(5540), 137–141.
30 A. K. Salem, P. C. Searson and K. W. Leong, Multifunctional nanorods for gene delivery, *Nat. Mater.*, 2003, **2**(10), 668–671.
31 B. Wildt, P. Mali and P. C. Searson, Electrochemical template synthesis of multisegment nanowires: fabrication and protein functionalization, *Langmuir*, 2006, **22**(25), 10528–10534.
32 H. M. Zhang, Y. G. Guo, L. J. Wan and C. L. Bai, Novel electrocatalytic activity in layered Ni-Cu nanowire arrays, *Chem. Commun.*, 2003, **24**, 3022–3023.
33 R. D. Groot and P. B. Warren, Dissipative particle dynamics: bridging the gap between atomistic and mesoscopic simulation, *J. Chem. Phys.*, 1997, **107**(11), 4423–4435.
34 D. Frenkel and M. Smit, *Understanding Molecular Simulation*, Academic Press, New York, 2002.
35 R. B. Bird, P. J. Dotson and N. L. Johnson, Polymer solution rheology based on a finitely extensible bead-spring chain model, *J. Non-Newtonian Fluid Mech.*, 1980, **7**(2–3), 213–235.
36 Y. J. Sheng, A. Z. Panagiotopoulos, S. K. Kumar and I. Szleifer, Monte-Carlo calculation of phase equilibria for a bead-spring polymeric model, *Macromolecules*, 1994, **27**(2), 400–406.
37 K. Kremer and G. S. Grest, Dynamics of entangles linear polymer melts: a molecular-dynamics simulation, *J. Chem. Phys.*, 1990, **92**(8), 5057–5087.
38 J. R. Silbermann, S. H. L. Klapp, M. Schoen, N. Chennamsetty, H. Bock and K. E. Gubbins, Mesoscale modeling of complex binary fluid mixtures: towards an atomistic foundation of effective potentials, *J. Chem. Phys.*, 2006, **127**(7), 074105-1–074117-12.

39 R. P. Carney, G. A. DeVries, C. Dubois, H. Kim, J. Y. Kim, C. Singh, P. K. Ghorai, J. B. Tracy, R. L. Stiles, R. W. Murray, S. C. Glotzer and F. Stellacci, Size limitations for the formation of ordered striped nanoparticles, *J. Am. Chem. Soc.*, 2008, **130**(3), 798–799.

40 B. P. Khanal and E. R. Zubarev, Rings of nanorods, *Angew. Chem., Int. Ed.*, 2007, **46**(13), 2195–2198.

41 Y. Hu, O. Uzun, C. Dubois and F. Stellacci, Effect of ligand shell structure on the interaction between monolayer-protected gold nanoparticles, *J. Phys. Chem. C*, 2008, **112**(16), 6279–6284.

42 Y. Hu, B. H. Wunsch, S. Sahni and F. Stellacci, Statistical analysis of scanning tunneling microscopy images of 'striped' mixed monolayer protected gold nanoparticles, *J. Scanning Probe Microsc.*, 2009, **4** (1), 24–35.

43 A. M. Jackson, Y. Hu, P. J. Silva and F. Stellacci, From homoligand- to mixed-ligand-monolayer-protected metal nanoparticles: a scanning tunneling microscopy investigation, *J. Am. Chem. Soc.*, 2006, **128**(34), 11135–11149.

44 A. Santos, C. Singh and S. C. Glotzer, Coarse-grained models of tethers for fast self-assembly simulations, *Phys. Rev. E: Stat., Nonlinear, Soft Matter Phys.*, 2010, **81**(1), 011113-1.

45 C. Singh, H. Ying, A. M. Jackson, F. Stellacci and S. C. Glotzer, Ordered nanoscale stripes and micelles in mixed self-assembled monolayers, in preparation.

46 C. Singh, A. M. Jackson, F. Stellacci and S. C. Glotzer, Exploiting substrate stress to modify nanoscale SAM patterns, *J. Am. Chem. Soc.*, 2009, **131**(45), 16377–16379.

47 K. L. Kohlstedt, F. J. Solis, G. Vernizzi and M. O. de la Cruz, Spontaneous chirality *via* long-range electrostatic forces, *Phys. Rev. Lett.*, 2007, **99**(3), 030602-1.

48 M. M. D. Lim, Y. S. Velichko, M. O. de la Cruz and G. Vernizzi, Low-radii transitions in co-assembled cationic - anionic cylindrical aggregates, *J. Phys. Chem. B*, 2008, **112**(17), 5423–5427.

49 F. J. Solis, S. I. Stupp and M. O. de la Cruz, Charge induced pattern formation on surfaces: segregation in cylindrical micelles of cationic-anionic peptide-amphiphiles, *J. Chem. Phys.*, 2005, **122**(5), 054905-1.

50 Y. S. Velichko and M. O. de la Cruz, Pattern formation on the surface of cationic-anionic cylindrical aggregates, *Phys. Rev. E: Stat., Nonlinear, Soft Matter Phys.*, 2005, **72**(4), 041920-1–041920-4.

51 G. Vernizzi, K. L. Kohlstedt and M. O. de la Cruz, The electrostatic origin of chiral patterns on nanofibers, *Soft Matter*, 2009, **5**(4), 736–739.

52 I. Langmuir, Monolayers on solids, *J. Chem. Soc.*, 1940, **94**, 511–543.

53 H. M. McConnell, L. K. Tamm and R. M. Weis, Periodic structures in lipid monolayer phase transitions, *Proc. Natl. Acad. Sci. U. S. A.*, 1984, **81**, 3249–3253.

54 H. M. McConnell and V. T. Moy, Shapes of finite two-dimensional lipid domains, *J. Phys. Chem.*, 1988, **92**, 4520–4525.

55 K. Y. Lee, J. F. Klingler and H. M. McConnell, Electric field-induced concentration gradients in lipid monolayers, *Science*, 1994, **263**(5147), 655–658.

56 S. L. Keller and H. M. McConnell, Stripe phases in lipid monolayers near a miscibility critical point, *Phys. Rev. Lett.*, 1999, **82**(7), 1602–1605.

57 S. Garoff, Molecularstructure of surfactant-coated surfaces, *Proc. Natl. Acad. Sci. U. S. A.*, 1987, **84**, 4729–4732, Letters 99:226106.

58 D. S. Zhang, M. A. Carignano and I. Szleifer, Cluster structure and corralling effect driven by interaction mismatch in two dimensional mixtures, *Phys. Rev. Lett.*, 2006, **96**, 028701.

59 M. Seul and D. Andelman, Domain shapes and patterns—the phenomenology of modulated phases, *Science*, 1995, **267**, 476–483.

60 D. Andelman, F. Brochard and J. F. Joanny, Modulated structures and competing interactions in Amphiphilic monolayers, *Proc. Natl. Acad. Sci. U. S. A.*, 1987, **84**, 4717–4718.

61 C. Park, J. Yoon and E. L. Thomas, Enabling nanotechnology with self assembled block copolymer patterns, *Polymer*, 2003, **44**, 6725–6760.

62 S. C. Glotzer and A. Coniglio, Self-Consistent solution of phase-separation with competing interactions, *Phys. Rev. E: Stat., Nonlinear, Soft Matter Phys.*, 1994, **50**, 4241–4244.

63 S. C. Glotzer, E. A. Dimarzio and M. Muthukumar, Reaction-controlled morphology of phase-separating mixtures, *Phys. Rev. Lett.*, 1995, **74**, 2034–2037.

64 S. C. Glotzer, D. Stauffer and N. Jan, Monte-Carlo simulations of phase-separation in chemically reactive binary-Mixtures, *Phys. Rev. Lett.*, 1995, **75**, 1675–1675.

65 C. B. Muratov, Instabilities and disorder of the domain patterns in systems with competing interactions, *Phys. Rev. Lett.*, 1997, **78**, 3149–3152.


 